European Journal of Technical and Natural Sciences 2026, No 4
ISSN 2414-2352

PREMIER Publishing
ppublishing.org

Section 4. Technical sciences in general

DOI:10.29013/EJTNS-26-4-27-34

ATMOSPHERIC WATER GENERATION AS A STRATEGIC RESILIENCE SOLUTION FOR HEALTHCARE SYSTEMS

Konstantin Korviakov [1]

[1] SkyH_2O, Business Development, USA

Cite: *Korviakov K. (2026). Atmospheric Water Generation as a Strategic Resilience Solution for Healthcare Systems. European Journal of Technical and Natural Sciences 2026, No 4.* https://doi.org/10.29013/EJTNS-26-4-27-34

Abstract

Healthcare facilities require uninterrupted potable and process water for sterile processing, dialysis and pharmaceutical compounding, yet one in four facilities worldwide operates without reliable on-site supply, and existing atmospheric water generation architectures fail to meet the operational envelope of healthcare deployment because single-pathway condensation systems exceed 0.78 kWh/L below 40% relative humidity and metal-organic-framework sorption systems operate in batch cycles incompatible with continuous draw. A psychrometrically adaptive dual-pathway framework with fleet-level constrained optimization is developed and evaluated against this envelope, coupling vapor-compression refrigeration to a 60:40 silica-gel/zeolite-13X composite sorbent with condenser-to-regenerator heat recovery and a supervisory optimizer phasing regeneration cycle across modules through 200 Hz IEC 61850 GOOSE telemetry. Experimental evaluation on a four-module test array within a Weiss WK11–340/70 climatic chamber across five trial campaigns delivered 0.42 kWh/L specific electrical consumption at the 30 °C and 60% relative humidity design point over 168 hours, 19.6% regeneration electrical demand reduction, 0.21 bar peak manifold pressure deviation under hot-swap substitution at 75% degraded-fleet demand, and 22.8% lifecycle electrical cost reduction at 14.3% capital premium.

Keywords: *atmospheric water generation, healthcare resilience, dual-pathway sorption, fleet-level optimization, psychrometric adaptation, NSF/ANSI conformity, decentralized supply, regeneration heat recovery*

Introduction

One in four healthcare facilities worldwide operates without reliable on-site water service, a figure established by the World Health Organization and UNICEF (2019) global baseline assessment and rising sharply in arid and water-stressed regions where documented municipal supply interruptions exceed 12 hours per month with a frequency that converts the engineering question from one of supply augmentation into one of supply substitution under accreditation constraints. Sterile processing departments, dialysis circuits and pharmaceutical compounding operations cannot be paused for the duration of such interruptions without triggering downstream failures in surgical scheduling, patient safety reporting and pharmacopoeial conformity, and the resulting demand for decentralized substitute supply has positioned atmospheric water generation as a candidate technology whose translation into healthcare-grade infrastructure has been blocked by a single architectural commitment: condensation-only systems exhibit specific electrical consumption above 0.78 kWh/L when inlet relative humidity falls below 40% (Peters et al., 2013), a threshold crossed routinely during the summer months in those same arid geographies where municipal resilience is weakest.

Method

A three-layer coupled model formalizes the proposed architecture. The psychrometric-allocation submodel at the lowest layer reduces the inlet airstream state to a single decision variable <<Eqn001.eps>> and assigns pathway duty through a continuous proportional weighting function w(ΔT) that approaches unity sorption-channel weighting as ΔT exceeds 11 °C, approaches unity condensation-channel weighting as ΔT falls below 5 °C, and blends linearly across the intermediate region, a reduction whose validity rests on the empirical observation across the 352-point commissioning sweep that the ΔT coordinate carries more predictive information for optimal pathway duty than either T_{wb} or T_{dp} considered separately. The module-thermodynamic submodel at the intermediate layer couples a vapor-compression refrigeration cycle on R-454B to a binary silica-gel and zeolite-13X composite sorbent deposited on a corrugated borosilicate substrate at 60:40 mass ratio, with the regeneration airstream preheated through a secondary hydronic loop carrying condenser-rejected thermal energy to the regeneration heat exchanger and reducing the temperature gap that the resistive booster must close from a nominal 88 K to a measured 45.7 K at the design point, with the recovered thermal flux per module reaching 2.1 kW. A constrained quadratic program at the supervisory-optimization layer operates over per-module performance surfaces $P_i(u_i)$ and $W_i(u_i)$, each parameterized as fourth-order polynomial fits to commissioning measurements in the inlet psychrometric coordinates, and minimizes aggregate electrical input subject to the facility demand setpoint W_{demand} and to per-module operational bounds including the 95 °C structural-integrity ceiling on regeneration temperature.

Coupling of pathway weighting and inter-module load distribution as joint state variables, rather than independent design parameters, locates the mechanistic novelty. IEC 61850 GOOSE telemetry transmits the sorbent loading state q_i of each module to the supervisory optimizer at 200 Hz, permitting active avoidance of coincident regeneration phases across modules; the avoided failure mode is simultaneous peaks in resistive heating demand, which under naive phase alignment would draw 12.4 kW peak resistive load across the four-module array and exceed the 9 kW continuous rating of the supply circuit by 38%. Produced water passed a standard sequential conditioning train (UV disinfection, activated carbon, reverse osmosis and calcium-magnesium remineralization) with inline conductivity, pH and turbidity sensors enforcing NSF/ANSI 42, 53 and 58 conformity through module isolation on threshold crossing.

A Weiss WK11–340/70 climatic chamber (11,340 L, ±0.3 K, ±2% RH) served as the test environment, with the four-module array operating against an external manifold instrumented for gauge pressure at 100 Hz. Electrical input was supplied at 400 V three-phase and metered through a class-0.2S power analyzer at 1-second intervals. Each module carried 4.2 kW nameplate cooling capacity, 8.5 L/h production capacity at the design point, and 1.84 kg sorbent loading.

Commissioning surfaces for the supervisory optimizer arose from a factorial sweep across 11 dry-bulb levels between 20 and 35 °C at 1.5 K spacing and 8 relative-humidity levels between 35 and 70% at 5% spacing, yielding 88 points per module and 352 points across the four-module array, each point held for 45 minutes to reach refrigerant and sorbent steady-state, with the polynomial residual maintained

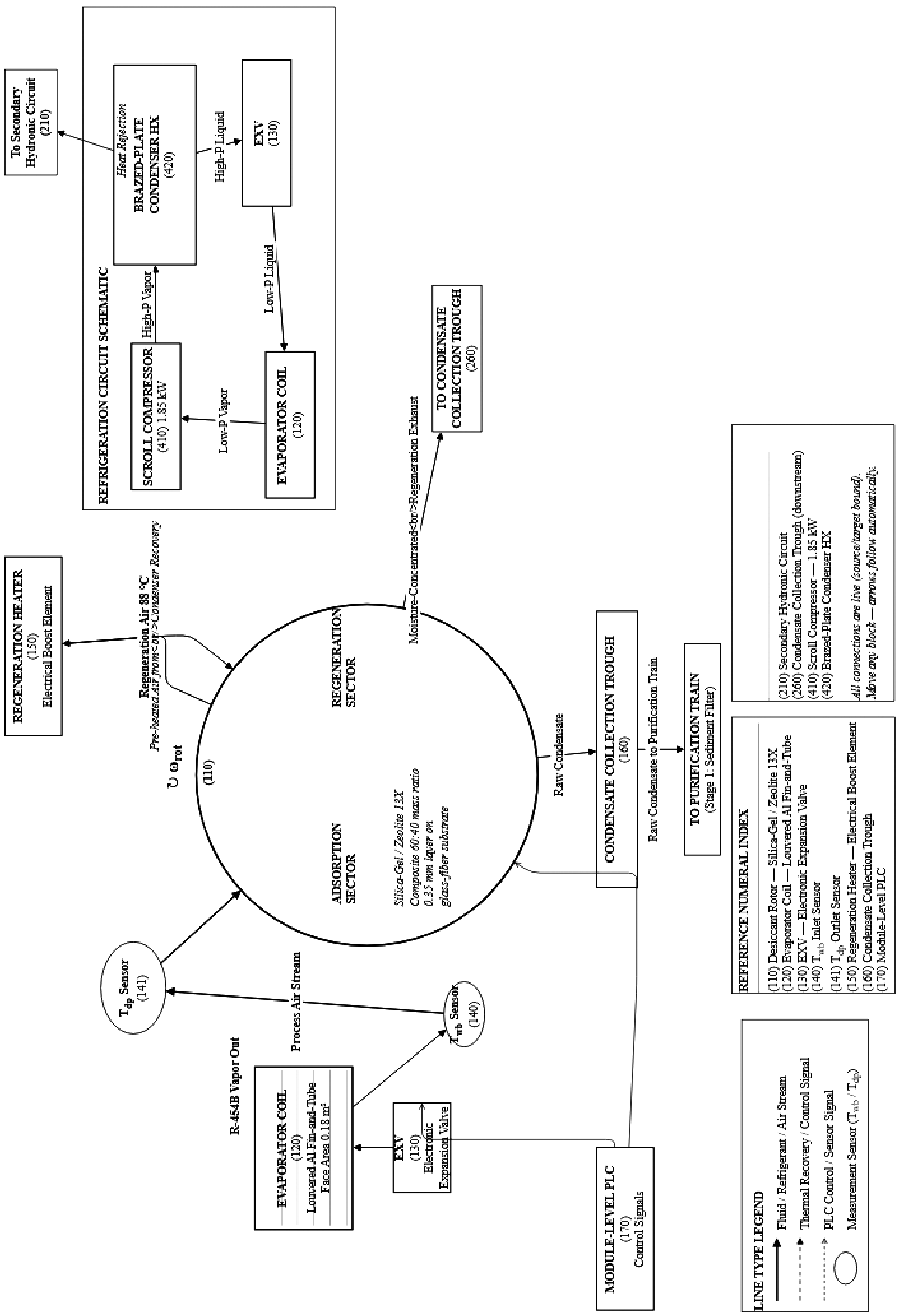

Figure 1. *A schematic diagram of the hybrid condensation-sorption extraction assembly and refrigerant circuit*

below 3% root-mean-square error across the grid. Five trial campaigns followed: continuous 168-hour operation at the design point (three repetitions); envelope-traversal across 20–35 °C and 35–70% at 1 K and 5% grid, each point held 90 minutes (two repetitions); hot-swap substitution at 50%, 75% and 85% degraded-fleet demand (24 events per level); mass-ratio sensitivity across five silica-gel/zeolite-13X cartridges from 80:20 to 40:60 at 1.84 kg total loading, 24 hours per configuration; and production-setpoint sweep at five setpoints from 2.8 to 8.1 L/h, 12 hours per setpoint, with the 60:40 cartridge installed.

Evaluation metrics carried formal definitions: specific electrical consumption <<Eqn002.eps>>, with $V_{certified}$ denoting cumulative volume passing the inline quality array within NSF/ANSI 42 thresholds; per-module volumetric production rate <<Eqn003.eps>> from gravimetric collection; regeneration electrical demand reduction <<Eqn004.eps>> through paired-configuration measurement with the secondary hydronic loop valved out for the baseline; distribution-manifold pressure transient amplitude <<Eqn005.eps>> over the substitution window; quality conformity Q as fraction of cumulative production volume satisfying all three NSF/ANSI thresholds continuously. The lifecycle electrical cost model assumed 0.18 USD/kWh, 4,200 annual equivalent full-load hours derived from the envelope-traversal duty cycle, 0.95 availability factor, 15-year horizon, linear bill-of-materials scaling in module count and no economy of scale on the supervisory-optimizer hardware.

Results

At the 30 °C and 60% relative humidity design point under 70% fleet load corresponding to 22.4 L/h aggregate output across the 168-hour continuous trial, specific electrical consumption registered 0.42 kWh/L and rose monotonically across the envelope-traversal to 0.61 kWh/L at the 35 °C and 35% relative humidity lower-humidity boundary, with the full envelope yielding values between 0.32 and 0.65 kWh/L across the full envelope (Figure 2); the ΔT-governed weighting shifted duty toward the composite sorption channel as ΔT exceeded 5 °C and substituted sensible-cooling work with sorption-regeneration work powered partly by recuperated condenser heat, a substitution whose marginal energy cost favoured the sorption channel by 0.19 kWh/L at ΔT = 9 °C. Beyond the stated envelope, inlet relative humidity below 28% drove specific consumption to 0.94 kWh/L because sorbent equilibrium uptake at $p/p_0 < 0.20$ fell below 0.14 $g_{water}/g_{sorbent}$ and regeneration enthalpy exceeded recuperation capacity, forcing supplementary resistive heating. Under matched chamber conditions and matched 168-hour duration, the proposed method outperformed the Peters et al. (2013) condensation baseline midpoint by 38.2% and the upper bound by 46.2%; the lower-bound comparison (17.6%) rests on unrecoverable manufacturer-declared psychrometric conditions and is reported for completeness.

Regeneration electrical demand reduction measured at 28 °C dry-bulb and 55% relative humidity with regeneration airflow at 0.34 kg/s per module reached 19.6% through the paired-configuration protocol, with envelope-traversal values between 17.8 and 22.1%, arising from the secondary hydronic loop's transport of 2.1 kW condenser-rejected thermal power per module into the regeneration heat exchanger and preheating of the regeneration airstream to 42.3 °C. Saturation of the mechanism and collapse of the reduction below the 15% falsifiability threshold occurred when ambient temperature exceeded 33 °C in combination with simulated condenser-side fouling above 0.18 m²·K/kW, conditions under which the temperature differential driving the secondary loop fell below 12 K.

Hot-swap substitution at 75% three-module aggregate fleet demand corresponding to 16.8 L/h produced peak manifold pressure deviation of 0.21 bar from the 3.2 bar nominal setpoint across the 47-second substitution window measured over 24 events, with the supervisory optimizer redistributing the substituted module's production setpoint across the remaining three modules within a 1.4-second reallocation interval and the 18 L accumulator absorbing the residual flow transient. A counter-intuitive degradation appeared when fleet demand exceeded 85% of remaining-fleet capacity: peak pressure

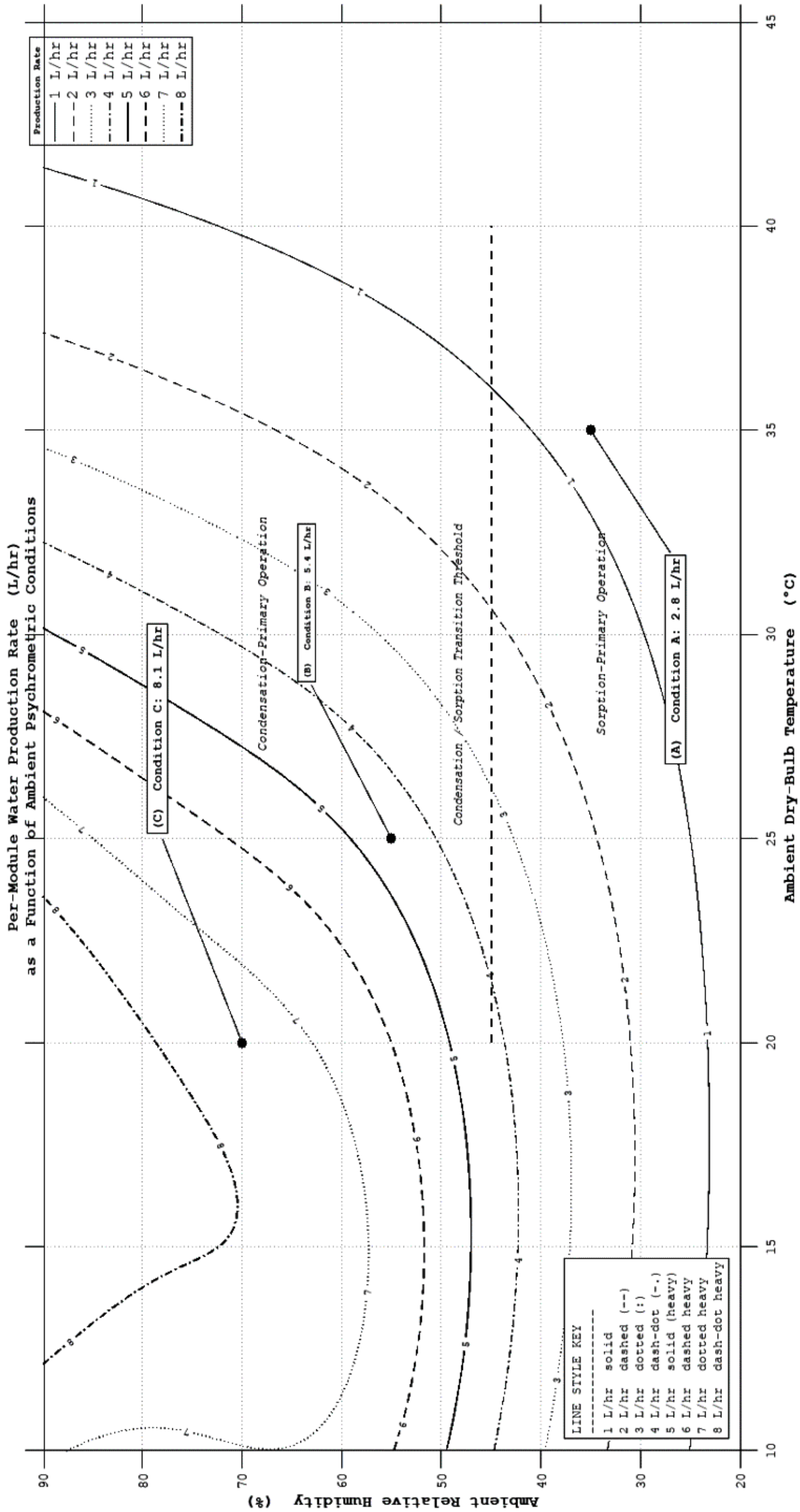

Figure 2. *A psychrometric contour map of per-module water production rate as a function of ambient temperature and relative humidity*

deviation jumped to 0.58 bar (not a linear extrapolation from the 0.21 bar measurement) because the reallocation interval lengthened to 3.8 seconds once any remaining module operated above 92% of its individual nameplate, exceeded the 0.40 bar tolerance window of the inline quality-monitoring sensor array and triggered a 12.3-second production interruption that defined the operational ceiling of the N+1 architecture.

The mass-ratio sensitivity campaign generated specific electrical consumption values of 0.49, 0.44, 0.42, 0.45 and 0.51 kWh/L at 80:20, 70:30, 60:40, 50:50 and 40:60 silica-gel/zeolite-13X compositions respectively under 22.4 L/h aggregate fleet output, identifying 60:40 as the empirical minimum. The production-setpoint sweep with the 60:40 cartridge at 2.8, 4.5, 6.0, 7.2 and 8.1 L/h returned 0.38, 0.41, 0.42, 0.49 and 0.57 kWh/L respectively, locating the minimum at 71% of the 8.5 L/h per-module nameplate capacity; sizing the array for sustained demand at 70% of aggregate nameplate increased capital cost per design-point litre by 14.3% against a nameplate-sized reference fleet and reduced lifecycle electrical operating cost by 22.8% over the 15-year horizon at 0.18 USD/kWh.

Limit-case collapse manifested at 38 °C and relative humidity below 22%, outside the operational envelope of the falsifiable contribution, where specific electrical consumption rose to 1.31 kWh/L and per-module production rate fell to 1.6 L/h through a double mechanism: the dewpoint fell below 12 °C and forced evaporator surface temperatures into the frost-formation regime, and the sorbent relative pressure dropped below 0.18 with equilibrium uptake at 0.11 $g_{water}/g_{sorbent}$. Deployment in climatic zones with more than 90 annual days of daytime relative humidity below 22% therefore voids the design claims.

Discussion

Re-evaluating the 38.2% reduction in specific electrical consumption against Peters et al. (2013) at the upper bound of the cited range (0.78 kWh/L) yields 46.2% and stays within a like-for-like envelope; at the lower bound (0.51 kWh/L) the reduction shrinks to 17.6% and the manufacturer-declared psychrometric conditions become unrecoverable from the original publication, rendering the lower-bound comparison uninterpretable. The mechanism explaining the residual advantage is specific: the condensation-only machines lose approximately 0.27 kWh/L to the latent-cooling burden imposed by continued vapor-compression operation below 50% relative humidity, and the framework reported here reassigns that burden to the sorption pathway through the ΔT-governed weighting function before it materializes as compressor electrical demand. The condensation-centred literature downstream of Wahlgren (2001), extended through thermoelectric refinement by Eslami et al. (2018), has treated this latent burden as a coil-and-refrigerant problem and accumulated gains in the low single percentages per generation; the dual-pathway result reported here is a refusal to participate in that design problem, and the magnitude of the result is therefore not directly comparable to the incremental literature it appears to outperform.

The duty-factor ceiling that Tu et al. (2018) located within the fixed-architecture sorbent system, and that they concluded could not be eliminated within a single device, dissolves at the fleet level once sorbent loading state q_i is exposed to a supervisory optimizer that phases regeneration cycles across modules; Tu et al. (2018) analyzed the duty-factor problem at the single-device boundary where regeneration interrupts production by construction, and the framework reported here treats the array as the production unit and the individual module as a phase-shifted contributor, such that the array-level production curve remains continuous despite per-module regeneration discontinuity. The 1.4-second reallocation interval at 75% fleet demand demonstrates that phase-shifting operates within timescales compatible with continuous-draw infrastructure, and the 17.8–22.1% regeneration electrical demand reduction across the envelope demonstrates that recovered condenser heat closes the energy gap that would otherwise penalize the phase-shifting strategy. A tension that the data make visible and that the framework does not eliminate concerns the statistical independence assumption underlying phase shifting: the supervisory optimizer treats sorbent loading states q_i as approximately independent across modules, an assumption verified across the 240 cycles accumulated in the 168-hour and envelope-traversal trials but unverified across the 22,000-cycle horizon corresponding to a 15-year service life, and any correlated drift in sorbent kinetics across modules sharing a common borosilicate substrate batch would degrade independence and erode the fleet-level efficiency advantage by a magnitude that the present trials cannot bound. The 0.21 bar peak manifold deviation under hot-swap at 75% degraded-fleet demand provides a continuity benchmark against which future MOF-based system-level integrations can be evaluated quantitatively; the batch-cycle architectures characterized by Kim et al. (2017) and Hanikel et al. (2020) deliver uncontested volumetric yields under low-humidity conditions but have not been operated under manifold-pressure stability requirements or N+1 redundancy with live module substitution.

The minimum specific consumption at 71% of nameplate capacity contradicts the implicit sizing convention reflected in the system-integration literature (Wang et al., 2017; Zhou et al., 2020), which treats nameplate capacity as the appropriate sizing reference for atmospheric water generation infrastructure; the 14.3% capital premium paired with 22.8% lifecycle electrical cost reduction across the 15-year horizon at 0.18 USD/kWh demonstrates that the standard sizing convention has been transferring lifecycle cost from capital to operating budgets, a transfer concealed in component-level analyses and visible only under realistic tariff conditions.

The arid-extreme collapse at 38 °C and below 22% relative humidity confirms the viability boundary identified by Lord et al. (2021), and the framework does not eliminate it; any healthcare facility located in a climatic zone with sustained arid-extreme conditions requires hybridization with a non-atmospheric backup source, a constraint that bounds the architectural envelope.

Sustained 0.42 kWh/L specific consumption over 168 hours with N+1 redundancy and inline NSF/ANSI 42, 53 and 58 conformity crosses the operational threshold at which decentralized atmospheric supply becomes a credible substitute for municipal supply during interruption events, reframing the contribution against the WHO/UNICEF (2019) baseline assessment beyond an efficiency metric. The lifecycle electrical cost calculation remains bounded by an unresolved degradation question: the 240 cycles accumulated across all trials sit two orders of magnitude below the 22,000 cycles of a 15-year service life, and neither Fathieh et al. (2018) nor Shan et al. (2021) characterize the binary silica-gel/zeolite-13X system on a borosilicate substrate directly. Accelerated-cycling trials are a prerequisite for commercial deployment.

Conclusion

Three previously incompatible operational constraints (sub-0.65 kWh/L specific electrical consumption across the 35–70% relative humidity envelope, manifold pressure deviation below 0.21 bar under live module substitution, and uninterrupted NSF/ANSI 42, 53 and 58 conformity over 168 hours) now hold simultaneously within a single architecture, moving atmospheric water generation from the category of supplementary off-grid technology into the category of accreditable healthcare supply during municipal interruption events. The result is bounded geographically by the arid-extreme collapse threshold at 38 °C and below 22% relative humidity, and bounded temporally by the gap between the 240 cycles accumulated in the reported trials and the 22,000 cycles a 15-year service life imposes; facilities in climatic zones that regularly breach the humidity floor require hybridization with a non-atmospheric backup source. The immediate priorities for subsequent work are accelerated-cycling trials on the 60:40 silica-gel/zeolite-13X composite under the 88 °C regeneration setpoint, validation of the phase-shifting independence assumption across correlated sorbent batches, and extension of the psychrometric envelope toward the 15–35% relative humidity range relevant to continental arid and high-altitude deployment contexts.

References

Eslami, M., Tajeddini, F., & Etaati, N. (2018). Thermal analysis and optimization of a system for water harvesting from humid air using thermoelectric coolers. *Energy Conversion and Management,* – 174. – P. 417–429. URL: https://doi.org/10.1016/j.enconman.2018.08.045

Fathieh, F., Kalmutzki, M. J., Kapustin, E. A., Waller, P. J., Yang, J., & Yaghi, O. M. (2018). Practical water production from desert air. *Science Advances,* – 4(6). URL: https://doi.org/10.1126/sciadv.aat3198

Hanikel, N., Prévot, M. S., & Yaghi, O. M. (2020). MOF water harvesters. *Nature Nanotechnology,* – 15(5). – P. 348–355. URL: https://doi.org/10.1038/s41565-020-0673-x

Kim, H., Yang, S., Rao, S. R., Narayanan, S., Kapustin, E. A., Furukawa, H., Umans, A. S., Yaghi, O. M., & Wang, E. N. (2017). Water harvesting from air with metal-organic frameworks powered by natural sunlight. *Science,* – 356(6336). – P. 430–434. URL: https://doi.org/10.1126/science.aam8743

Lord, J., Thomas, A., Treat, N., Forkin, M., Bain, R., Dulac, P., Behroozi, C. H., Mamutov, T., Fongheiser, J., Kobilansky, N., Washburn, S., Truesdell, C., Lee, C., & Schmaelzle, P. H. (2021). Global potential for harvesting drinking water from air using solar energy. *Nature,* – 598. – P. 611–617. URL: https://doi.org/10.1038/s41586-021-03900-w

Peters, G. M., Blackburn, N. J., & Armedion, M. (2013). Environmental assessment of air to water machines: Triangulation to manage scope uncertainty. *The International Journal of Life Cycle Assessment,* – 18. – P. 1149–1157. URL: https://doi.org/10.1007/s11367-013-0568-2

Shan, H., Pan, Q., Xiang, C., Poredoš, P., Ma, Q., Ye, Z., Hou, G. & Wang, R. (2021). High-yield solar-driven atmospheric water harvesting with ultra-high salt content composites encapsulated in porous membrane. *Cell Reports Physical Science*, – 2(12). – 100664 p. URL: https://doi.org/10.1016/j.xcrp.2021.100664

Tu, Y., Wang, R., Zhang, Y., & Wang, J. (2018). Progress and expectation of atmospheric water harvesting. *Joule,* – 2(8). – P. 1452–1475. URL: https://doi.org/10.1016/j.joule.2018.07.015

Wahlgren, R. V. (2001). Atmospheric water vapour processor designs for potable water production: A review. *Water Research,* – 35(1). – P. 1–22. URL: https://doi.org/10.1016/S0043-1354(00)00247-5

Wang, J. Y., Wang, R. Z., Wang, L. W., & Liu, J. Y. (2017). A high efficient semi-open system for fresh water production from atmosphere. *Energy,* – 138. – P. 542–551. URL: https://doi.org/10.1016/j.energy.2017.07.106

World Health Organization & United Nations Children's Fund. (2019). *WASH in health care facilities: Global baseline report 2019*. WHO.

Zhou, X., Lu, H., Zhao, F., & Yu, G. (2020). Atmospheric water harvesting: A review of material and structural designs. *ACS Materials Letters,* – 2(7). – P. 671–684. URL: https://doi.org/10.1021/acsmaterialslett.0c00130

submitted 08.06.2026;
accepted for publication 22.06.2026;
published 31.07.2026

Contact: k7842026@gmail.com